Biomaterials 78 (2016) 50–61

Contents lists available at ScienceDirect

Biomaterials

journal homepage: www.elsevier.com/locate/biomaterials

Modelling the tumour microenvironment in long-term microencapsulated 3D co-cultures recapitulates phenotypic features of disease progression

Marta F. Estrada [a, b], Sofia P. Rebelo [a, b], Emma J. Davies [c, d], Marta T. Pinto [e], Hugo Pereira [a, f], Vítor E. Santo [a, b], Matthew J. Smalley [c], Simon T. Barry [d], Emilio J. Gualda [f], Paula M. Alves [a, b], Elizabeth Anderson [g], Catarina Brito [a, b, *]

[a] iBET, Instituto de Biologia Experimental e Tecnológica, Oeiras, Portugal
[b] Instituto de Tecnologia Química e Biológica António Xavier, Universidade Nova de Lisboa, Oeiras, Portugal
[c] European Cancer Stem Cell Institute, Cardiff University, Cardiff, UK
[d] Bioscience, Oncology iMed, AstraZeneca, Cheshire, UK
[e] Institute of Molecular Pathology and Immunology, University of Porto (IPATIMUP), Portugal
[f] Cell Imaging Unit, Instituto Gulbenkian de Ciência, Oeiras, Portugal
[g] Boehringer Ingelheim RCV, Wien, Austria

ARTICLE INFO

Article history:
Received 18 August 2015
Received in revised form
16 November 2015
Accepted 17 November 2015
Available online 19 November 2015

Keywords:
3D
Co-culture
Alginate microencapsulation
Stirred-tank bioreactors
Tumour microenvironment
Tumour progression

ABSTRACT

3D cell tumour models are generated mainly in non-scalable culture systems, using bioactive scaffolds. Many of these models fail to reflect the complex tumour microenvironment and do not allow long-term monitoring of tumour progression. To overcome these limitations, we have combined alginate microencapsulation with agitation-based culture systems, to recapitulate and monitor key aspects of the tumour microenvironment and disease progression. Aggregates of MCF-7 breast cancer cells were microencapsulated in alginate, either alone or in combination with human fibroblasts, then cultured for 15 days. In co-cultures, the fibroblasts arranged themselves around the tumour aggregates creating distinct epithelial and stromal compartments. The presence of fibroblasts resulted in secretion of pro-inflammatory cytokines and deposition of collagen in the stromal compartment. Tumour cells established cell–cell contacts and polarised around small lumina in the interior of the aggregates. Over the culture period, there was a reduction in oestrogen receptor and membranous E-cadherin alongside loss of cell polarity, increased collective cell migration and enhanced angiogenic potential in co-cultures. These phenotypic alterations, typical of advanced stages of cancer, were not observed in the mono-cultures of MCF-7 cells. The proposed model system constitutes a new tool to study tumour-stroma crosstalk, disease progression and drug resistance mechanisms.

1. Introduction

The tumour microenvironment is composed of cancer cells, fibroblasts, endothelial cells, immune cells and extracellular matrix (ECM), whose interactions are critical for tumour initiation and progression [1]. Tumour cells can induce a phenotypic change in healthy fibroblasts to become cancer associated fibroblasts (CAFs) with cancer-promoting properties such as secretion of matrix components (collagen and fibronectin), growth and inflammation factors [1]. Abnormal deposition of collagen has been associated with cancerous states due to increased matrix stiffness which is known to contribute to tumour cell dissemination [2]. Additionally, the activated stromal cells promote tumour progression by stimulating cancer cell proliferation and migration, and ultimately tumour metastasis [3]. Infiltrating stromal cells in the tumour are the main providers of matrix metalloproteinases (MMPs) that, through remodelling of ECM, release chemotactic agents and loosen the matrix contributing to tumour cell dissemination [4]. These changes are responsible for the recruitment of immune cells and for increasing chronic inflammation, which also contributes to tumour aggressiveness [5].

* Corresponding author. iBET, Apartado 12, 2780-901 Oeiras, Portugal.
E-mail address: anabrito@itqb.unl.pt (C. Brito).

http://dx.doi.org/10.1016/j.biomaterials.2015.11.030

In an attempt to mimic the complexity of the tumour microenvironment, many *in vitro* models have been developed in the recent years [6]. In most of these models however, tumour cells are grown as monotypic cultures in two-dimensions (2D). In 2D, cells are not able to organize into tissue-like structures since they lack the tridimensionality (3D) bestowed by the surrounding microenvironment [7]. In contrast, heterotypic tumour aggregate 3D cultures enable tumour cells to establish cell–cell and cell-ECM interactions, which are important elements in tumour signalling and which modulate tumour responses to therapeutic agents [8]. However, tumour aggregates are mostly cultured in low-adherence conditions [9] or embedded in bioactive scaffolds such as collagen I or matrigel [6]. These scaffolds also have limitations, including batch-to-batch variation and an incomplete understanding of their impact on cell behaviour [10,11]. In contrast, hydrogels such as alginate present many advantages over bioactive scaffolds due to their inert properties, biocompatible gelation and ease of cell recovery. Hydrogels also provide the possibility of conjugation with defined adhesion ligands or delivery of specific biomolecules (growth factors, pro-angiogenic factors, amongst others) [12,13].

Alginates are polysaccharide hydrogels composed of β-D-mannuronic acid (M) and α-L-guluronic acid (G) obtained from particular brown algae species [13]. Alginate comprises 99% water, but still retains high plasticity and mechanical strength. Gelling occurs almost instantaneously by cross-linking with divalent ions, like Ca^{2+}, allowing for cell entrapment under physiological conditions and rapid cell recovery by gel dissolution [14]. Most cell lines are able to grow in non-functionalized alginates, despite the absence of cell adhesion sites [13]. Alginate microencapsulation has been used to investigate the effect of biomechanical forces exerted on tumour aggregates [15]. More recently, alginate microencapsulation and microfluidic devices have been used to study the interaction between different cell types [11,16]. However, these models have been generated in non-scalable culture systems, with no control of the physicochemical parameters and which allow end-point analysis only [17,18]. As a result, studies on the molecular mechanisms behind disease progression and drug resistance as well as high-throughput drug screening are performed in models that lack the complexity of human tumours and which do not allow continuous monitoring of the culture progression.

Herein, we describe a novel *in vitro* culture model system for long-term co-culture of tumour and stromal cells, based on the combination of alginate microencapsulation with suspension cultures in agitation-based culture systems. We used alginate as a scaffold for cell entrapment, not only due to its properties outlined above, but also to provide physical support and cell confinement, in a manner compatible with stirred-tank systems. This strategy provides a means of long-term culture of tumour cell aggregates either alone or in combination with fibroblasts, continuously monitored with non-destructive sampling. The developed model system can be transferred across several pathologies and will provide a new tool for characterization of disease progression and drug resistance mechanisms *in vitro*.

2. Materials and methods

2.1. 2D cell culture

MCF-7 cells transduced with the lentiviral vectors PGK-dsRED and pCDH-CMV-MCS-EF1-Puro, were kindly provided by Professor Cathrin Brisken (EPFL, Switzerland) within the scope of the PREDECT consortium. MCF-7 reporter cells were used as a complementary tool for live monitoring purposes. Cell expansion was performed in Dulbecco's Modified Eagle Medium (DMEM) with 25 mM Glucose, supplemented with 1% (v/v) penicillin-streptomycin, 4 mM Glutamax, 1 mM sodium pyruvate and 10% (v/v) fetal bovine serum (FBS). Cells were passaged twice weekly at a inoculum concentration of 1.5×10^4 cell/cm^2. Human Dermal Fibroblasts (HDF), from Innoprot, were passaged once weekly for up to 10 to 12 passages at a seeding density of 0.5×10^4 cell/cm^2, in Iscove's Modified Dulbecco's Medium (IMDM) supplemented with 1% (v/v) penicillin-streptomycin and 10% (v/v) FBS (all from Life Technologies). Both the MCF-7 cells and the HDFs were cultured in static culture systems, in an incubator at 37 °C with humidified atmosphere containing 5% CO_2 in air.

2.2. 3D cell culture

MCF-7 cells, non transduced and transduced with the lentiviral vectors described above, were inoculated as single cell suspensions (0.2×10^6 cell/mL) into 125 mL stirred-tank vessels with flat centred cap and angled side arms (Corning – http://catalog2.corning.com/LifeSciences/en-US/Shopping/ProductDetails.aspx?categoryname=&productid=4500-125%28Lifesciences%29) and cultured at 80 rpm, to induce cell aggregation. For alginate microencapsulation, tumour cell aggregates were collected from the stirred-tank vessels after 24 h of culture. Aggregates corresponding to approximately 25×10^6 tumour cells were dispersed in 3 mL of 1.1% (w/v) of Ultrapure Ca^{2+} MVG alginate (UP MVG NovaMatrix, Pronova Biomedical, Oslo, Norway) dissolved in NaCl 0.9% (w/v) solution either alone (mono-cultures) or together with HDFs, in a 1:1 ratio for approximately 50×10^6 total cells (co-cultures). Mono-cultures of HDFs were also microencapsulated (25×10^6 total cells) and used as controls. Microencapsulation was performed using an electrostatic bead generator (Nisco VarV1, Zurich, Switzerland), to produce beads of approximately 500 μm in diameter [19]. The alginate droplets were cross-linked in a 100 mM $CaCl_2$/10 mM HEPES (pH 7.4) solution for 10 min, further washed three times in a 0.9% (w/v) NaCl solution and finally equilibrated in culture medium before being transferred to stirred-tank vessels. The microencapsulated mono and co-cultures were kept in 125 mL stirred-tank vessels at 80 rpm, in a humidified incubator, with 5% CO_2 in air, for 15 days with 50% medium exchange every 3–4 days.

2.3. Cell viability

Cell viability was assessed using fluorescein diacetate (FDA; Sigma–Aldrich) at 10 μg/mL to label live cells, and To-PRO-3 iodite (LifeTechnologies) at 1 μM, for dead cells. Microencapsulated tumour aggregates and fibroblasts were incubated for 5 min at RT with the labels then visualized using a fluorescence microscope (DMI6000, Leica Microsystems GmbH, Wetzlar, Germany) or a spinning disk microscope (Andor Revolution Å~ D, Andor Technology PLC, Belfast, Northern Ireland).

2.4. Aggregate size

To measure aggregate size, alginate microcapsules were dissolved in a chelating solution (Sodium citrate 50 mM/Sodium chloride 100 mM), for 5 min at room temperature (RT), and washed twice with Phosphate-Buffered Saline (PBS; Life Technologies). Aggregates were imaged using a fluorescence microscope (DMI6000, Leica Microsystems GmbH, Wetzlar, Germany). Aggregate surface area was quantified using FIJI open source software (Rasband, WS, ImageJ, U. S. National Institutes of Health, Bethesda, MD, USA, http://imagej.nih.gov/ij/, 1997–2012.), by applying automated threshold adjustment followed by the area measurement algorithm.

Statistical analysis was carried out using GraphPad Prism 5 software. Data is presented as mean ± SD from three independent

experiments. The non-parametric Kruskal–Wallis statistics test was used to compare aggregate surface area differences between mono and co-cultures, at days 2, 5, 10 and 15.

2.5. Total cell concentration

To assess cell concentration, alginate microcapsules were firstly dissolved, as described in the previous section. After dissolution of alginate, aggregates were pelleted by centrifugation at 50x *g* for 5 min at RT. Cells were lysed with 0.1 M of citric acid/1% (w/v) Triton − X100 in water. After cell lysis, nuclei were stained with 0.1% (v/v) Crystal Violet and counted in a Fuchs-Rosenthal haemacytometer chamber, using a phase contrast microscope (DMIRB, Leica, Germany).

Statistical analysis was carried out using GraphPad Prism 5 software. Data is presented as mean ± SD from four independent experiments. A two way ANOVA statistics test of significance was used to compare tumour cell growth in mono and co-cultures over time.

2.6. Immunofluorescence (IF) microscopy and image analysis

Culture samples were collected at days 5 and 15 of culture and fixed in 4% (v/v) paraformaldehyde (PFA)/4% (v/v) Sucrose for 20 min. For cryosectioning samples were dehydrated with 30% (w/v) sucrose overnight, frozen at −80 °C in Tissue-Tek O.C.T. (Sakura, Alphen aan den Rijn, Netherlands) and sectioned at a thickness of 10 μm using a cryomicrotome (Cryostat I, Leica, Wetslar, Germany).

Immunofluorescence was performed according to previously published methods [19,20]. In brief, cells were permeabilized with 0.1% Triton X-100 (w/v) (10 min for cryosections; 2 h for whole aggregates) and blocked in 0.2% (w/v) Fish Skin Gelatin (FSG; Sigma–Aldrich). Primary antibodies were diluted in 0.2% (w/v) FSG and incubated for 2 h at RT and secondary antibodies diluted in 0.125% (w/v) FSG and incubated for 1 h at RT (Supplementary Table 1). Samples were mounted in ProLong Gold Antifade Mountant containing DAPI (Life Technologies) and visualized using either a fluorescence microscope (DMI6000, Leica Microsystems GmbH, Wetzlar, Germany, a 2-photon microscope (Prairie TPE) or a Light Sheet Microscope (SPIM-FLUID).

2.7. Image acquisition and analysis in SPIM-FLUID

In order to facilitate automated sample loading, we used a system based on light-sheet fluorescence microscopy (LSFM), SPIM-Fluid [21]. Across a water filled chamber, at 45°, a FEP tube positioned at the intersection of the illumination and detection focal plane transports the samples, which can be aspired and pushed back and forward with an Arduino controlled stepper motor attached to a syringe (Eppendorf CellTram). Images are acquired sequentially, as the samples cross the light-sheet plane. The illumination block consists of a home-made laser combiner including two laser lines: 473 nm (DPSSL MBL-III-473-50) and 561 nm (Coherent OBIS 561-50 LS), selected using an Arduino controlled filter wheel with two filters (Semrock 473/10, 561/10). Laser scanning is carried out in the vertical axis using an Arduino controlled galvanometric mirror (6210H Cambridge Technologies) in which the optical plane is conjugated with the back focal aperture of an objective lens (Plan Fluor 4 × 0.13 WD17.4 mm) using a 3.5 × telescope system. For detection, an air objective (Nikon 10 × 0.3NA WD 16.7 mm), placed perpendicularly to the excitation plane, is used to collect fluorescence emission. Excitation light is rejected using emission filters placed in infinity space before the camera. Finally a 200 mm tube lens creates the image on the chip of the sCMOS cameras (Hamamatsu Orca-Flash4).

A controller for sample positioning and scanning allows microsteps up to 0.225°, which translate into sample steps of 2 microns (FEP tube of 1 mm inner diameter). To automatise the acquisition process, we have designed a photometer using a photodiode to detect sample passage. The system also permits control of a secondary camera, allowing fast two colour imaging. We have also created a dedicated java Plugin for Micromanager acquisition software [22], which enables easy control of sample positioning and data acquisition from a single window, creating a modular open source platform for high throughput screening on 3D cell cultures.

After image acquisition, images were processed using a kit of tools from FIJI image processing software [23]. In first place, data were sorted by image intensities in order to separate individual capsules. Subsequently, images having 2 capsules were processed with a different set of FIJI's tools to separate correctly the capsules and different aggregates per capsule in order to accurately estimate aggregate volume. Finally we used Image J plugins, such “3D Objects Counter”, “Analyze Particles” and “3D Manager”, to measure aggregate volume, fibroblast numbers and circularity.

2.8. Immunohistochemistry (IHC) and image analysis

Samples were collected and fixed as described above. Aggregates were pelleted, embedded in 1% (w/v) high melting temperature agarose (Lonza), dehydrated in graded alcohols and then embedded in paraffin wax. Paraffin blocks were sectioned (3 μm) for Hematoxylin & Eosin and immunohistochemical staining. Immunohistochemistry was carried out using standard protocols [24]. Briefly, antigen retrieval was performed using histoprocessing modules (Milestone Medical) at 110 °C under pressure, for 2 min, using pH6 antigen retrieval solution (Dako). Staining was performed using a Labvision Autostainer 720 (Thermo Scientific). Stained slides were scanned using a ScanScope AT Turbo slide scanner (Aperio) and images were analysed using Aperio image analysis software (Aperio). Aperio image analysis software is able to recognise either nuclear or membrane specific staining, and was trained to discern between negative, weak, medium and strong staining intensities.

Statistical analysis was carried out using GraphPad Prism 5 software. Data is presented as mean ± SD from more than 70 aggregates. Two-way ANOVA statistics test was used to compare the intensity of membranous E-cadherin and ER staining, in both mono and co-cultures, at days 5 and 15 of culture.

2.9. Western Blot (WB)

Culture samples were collected and alginate microcapsules dissolved, as described above in section 2.4. Following 2 steps of aggregate washing, cell pellets were snap frozen and stored at −80 °C. For Western Blot analysis aggregates were lysed in Tx-100 lysis buffer (50 mM Tris, 5 mM EDTA, 150 mM NaCl, 1% (w/v) Triton X-100 and 1x (w/v) complete protease and phosphatase inhibitor cocktail (Roche)). Protein quantification was performed using the Micro-BCA Protein Assay Kit (Thermo Scientific). Proteins were denatured, loaded in an electrophoresis gel (NuPAGE 4–12% Bis–Tris Gel) under reducing conditions for 40 min (200 V, 400 mA) and then electrophoretically transferred to a polyvinylidene fluoride (PVDF) membrane (Millipore). Membranes were blocked for 1 h in PBS with 0.1% (w/v) Tween 20/5% (w/v) non-fat dried milk powder and further incubated with the primary and secondary antibodies. Anti-β tubulin was used as a loading control. Membranes were developed using Amersham ECL Prime Western Blot Detection Reagent (GE Healthcare) and visualized using a Chem-iDocTM XRS + System (BioRad). Chemifluorescence was quantified

using Quantity One (Bio-rad).

Statistical analysis was carried out using GraphPad Prism 5 software. Data is presented as mean ± SD from three independent experiments. Two-way ANOVA statistics test was used to compare the average protein levels of ER, in both mono and co-cultures, at days 5 and 15 of culture.

2.10. Collagen quantification

Collagen was quantified in both alginate microcapsules and culture supernatants, using the Sircol Collagen Colorimetric assay kit (Biocolor Ltd., U.K.), according to the manufacturer's instructions.

Statistical analysis was carried out using GraphPad Prism 5 software. Data is presented as mean ± SD from three independent experiments. The non-parametric Kruskal–Wallis statistics test was used to compare collagen concentration between mono and co-cultures, at days 5 and 15.

2.11. Cytokine arrays

Culture samples were collected and alginate microcapsules were pelleted by centrifugation at 50x *g* and dissolved as described above. The microcapsule soluble fraction (MSF) was separated from the cell fraction by centrifugation. Cells and cell debris were removed from both culture supernatant (CS) and the MSF by additional centrifugation at 300x *g* followed by 1000x *g* for 5 min at 4 °C.

After concentration and buffer exchange of MSF to 1 mL, using centrifugal filter units with a 3 kDa membrane cut off (Amicon, Millipore), cytokine array analysis was performed using the Human Cytokine Array, Panel A (R&D Systems; ARY005), according to the manufacturer's instructions. Membranes were exposed to X-Ray films for 1, 5 and 10 min. The developed films were digitalized at 600 dpi using LabScan 5 Software (Amersham Biosciences, Switzerland). Spot analysis was performed using the Progenesis SameSpots software, version 4.5 (NonLinear Dynamics, UK). All films were quality checked, aligned and spots were quantified based on the volume and area of each spot. Relative secretion of each cytokine was calculated according with the following equation [25]:

$$Relative\,secretion\,(\%) = \frac{Cytokine\,secretion - negative\,control}{positive\,control - negative\,control} \times 100\%$$

Statistical analysis was carried out using GraphPad Prism 5 software. Data is presented as mean ± SD from two independent experiments. The non-parametric Man-Whitney U statistics Test (two-tailed p-value) was used to compare the cytokines present in culture supernatant vs MSF and the differences between mono and co-cultures; all comparisons were performed at days 5 and 15. Microencapsulated mono-cultures of fibroblasts were used as controls.

2.12. Chicken embryo chorioallantoic membrane (CAM) angiogenesis assay

The chicken embryo chorioallantoic membrane (CAM) assay was used to evaluate the angiogenic response to tumour aggregates from mono and co-cultures collected at day 15 of culture. Fertilized chicken (*gallus gallus*) eggs, obtained from commercial sources, were incubated horizontally at 37.8 °C in a humidified atmosphere. On embryonic day (E) 3 a square window was opened in the shell after removal of 2–2.5 mL of albumen, to allow detachment of the developing CAM. The window was sealed with adhesive tape and the eggs returned to the incubator. To remove the fibroblasts, ECM and soluble factors, alginate microcapsules were dissolved, as described above, and tumour aggregates were washed twice with PBS (Ca^{2+}/Mg^{2+}). Tumour aggregates were re-suspended in 10 μl of medium and placed in a 3 mm silicone ring on the E10 growing CAM (1×10^6 cell per embryo) under sterile conditions. The eggs were re-sealed and returned to the incubator for 3 days. After removing the ring, the CAM was excised from the embryos, photographed ex-ovo under a stereoscope, at 20x magnification (Olympus, SZX16 coupled with a DP71 camera).

The number of new vessels (less than 15 μm in diameter) growing radially towards the ring area, in which the cells had been applied to the CAM, were counted blinded. Statistical analysis was carried out using GraphPad Prism 5 software. Data is presented as mean ± SD from 18 eggs. A t- Test (two-tailed p-value) was used to test significance.

3. Results

3.1. Alginate microencapsulation combined with stirred-tank culture for long-term 3D heterotypic cell culture

To establish microencapsulated cultures, a dual step strategy in a stirred-tank culture system was adopted (Fig. 1). In the first stage, tumour cells were inoculated as single cell suspensions and cultured for 24 h to induce cell aggregation. Tumour aggregates were then collected (see materials and methods for details) and microencapsulated in alginate either alone (mono-culture) or together with human fibroblasts (tumour-stromal co-cultures), and further cultured in stirred-tank vessels for up to 15 days (Fig. 1). This strategy has been applied to both breast and lung cancer cell lines. The ability to sample in a non-destructive manner, offered by this system, allowed us to continuously monitor the culture progression and to take samples throughout the culture period without sacrificing the whole culture vessel. All cell types maintained viability throughout the duration of culture nonetheless cell growth kinetics and aggregate morphology varied from cell line to cell line. More specifically, whereas the MCF-7 breast cancer cell line only presented a significant increase in cell concentration during the first 6 days of culture, cell concentration of the lung cancer cell line NCI-H157 continued to increase throughout the 15 days of culture (data not shown). ER^+ breast cancers are described to present high frequency of disease relapse associated with metastasis and drug resistance, despite the initial response to endocrine therapy [27,28]. MCF-7 cells, one of the most widely used ER^+/PR^+ cell lines [29] were chosen as the focus of Work Package 1 of the PREDECT consortium (www.predect.eu) and therefore were used herein for characterization of our model system.

3.2. MCF-7 cell proliferation and partial polarisation, in microencapsulated cultures

Live/dead assays showed MCF-7 aggregates with circular morphology, defined edges, high cell viability and the absence of necrotic centres in both mono and co-cultures (Fig. 2A).

After an initial growth phase, up to day 6, MCF-7 cell number reached a plateau that remained constant until day 15 of culture (Fig. 2B). A slight increase in tumour cell concentration was observed in co-cultures by day 15, but this was not statistically significant. Aggregates from both culture types (mono and co-cultures) contained small lumina surrounded by polarised cells, as shown by apical accumulation of f-actin and ZO-1 (Fig. 2C1 and 2C2), together with pyknotic nuclei within the lumens (Fig. 2C3). Partial cell polarisation was seen at the outer rim of the aggregates as indicated by ZO-1 apical accumulation. Tumour cells were also cytokeratin 18 (CK18) positive, with localisation of E-cadherin

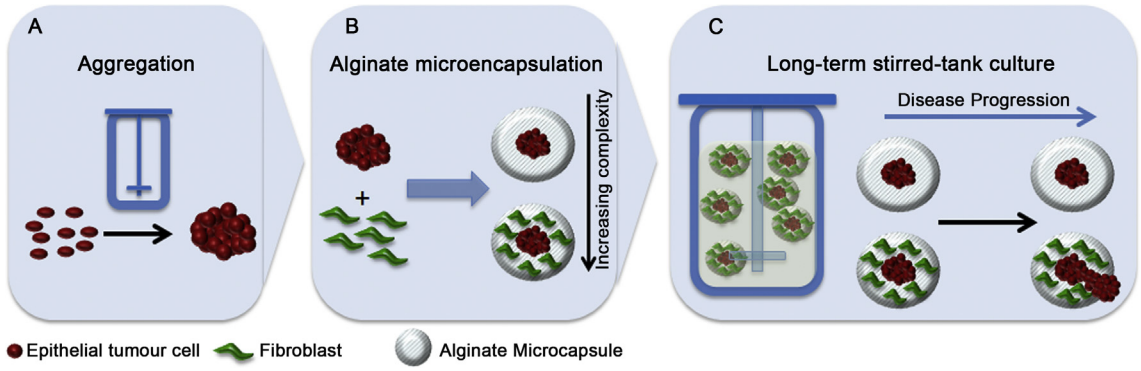

Fig. 1. Schematic illustration of the experimental approach – *in vitro* reconstruction of tumour microenvironment in stirred-tank culture systems. (A) MCF-7 cells were aggregated in stirred-tank vessels for 24 h and then harvested and pelleted for further microencapsulation. (B) Tumour aggregates were microencapsulated in alginate alone (tumour mono-cultures) or together with fibroblasts (tumour – stromal co-cultures). (C) Microencapsulated cells were cultured in stirred-tank vessels for up to 15 days during which culture characterization was carried out.

(Figure S1) and β-catenin (Fig. 2) at the cell membranes. In contrast, in non-microencapsulated cultures, tumour cells did not polarise, although cell–cell adhesions through E-cadherin were formed and CK18 expression was maintained (Figure S1). Additionally, proliferation (Ki67) and apoptosis (as indicated by caspase cleaved CK18 or M30) markers showed that proliferating cells were distributed homogeneously through the aggregates and that the number of apoptotic cells was very low. No apoptotic cell centres were detected in the aggregates. Overall, no phenotypic differences were observed between microencapsulated mono and co-cultures, until day 5 of culture.

3.3. Cell organization and collagen accumulation in alginate microcapsules resemble structures observed in human tumours

Immunofluorescence analysis by Light Sheet Microscopy of alginate microcapsules from co-cultures showed that fibroblasts were distributed around tumour aggregates (Fig. 3A), creating a "stromal compartment".

In non-microencapsulated cultures, fibroblasts accumulated in the centre of the aggregate [26]. Quantification of the number of fibroblasts *per* microcapsule, demonstrated that the number of fibroblasts was similar across microcapsules, that fibroblast concentration remained constant throughout the culture time (Fig. 3B). Vimentin and collagen (Type I and IV) expression was kept throughout the culture time (data not shown).

A 1.5-fold increase in collagen concentration was found in co-cultures at day 15 as compared to day 5. Furthermore, comparison of both types of culture revealed that the co-cultures had accumulated significantly higher levels of collagen than mono-cultures by day 15 (Fig. 3D). Using whole mount immunofluorescence of the microencapsulated co-cultures, we observed that collagen I accumulated in the stromal compartment (Fig. 3C) and assembled into fibres (Fig. 3C1), as typically observed in tissues [30].

3.4. The effect of stroma on disease progression events can be monitored and further investigated in long-term stirred-tank cultures

At day 15, aggregates in co-cultures presented an altered phenotype in that there was loss of aggregate circularity (Fig. 4A) and unidirectional aggregate migration from the microcapsules (Fig. 4B). Whilst in mono-cultures, 90% of the aggregates maintained the circularity observed at day 5 (95% in both cultures), in the co-cultures, the aggregate population became very heterogeneous, with 40% of the aggregates presenting an altered shape (Fig. 4A). These alterations were reflected in a significant increase in aggregate size between days 10 and 15 (Fig. 4C). Additionally, the co-culture aggregates were less compact, cell–cell contacts were decreased and cell polarity was lost in the surfaces of the lumens, as indicated by ZO-1 translocation to the cytoplasm (Fig. 4D). In contrast, the mono-cultures kept their initial phenotype throughout the culture period.

Oestrogen Receptor (ER) and E-cadherin protein expression and localisation in the aggregates were assessed by IHC and by WB (Fig. 5). At day 5, the proportion of cells showing strong nuclear ER staining was significantly lower in the co-cultures compared to the mono-cultures but did not reduce further over the culture period (Fig. 5A). The proportion of tumour cells in the mono-cultures showing strong ER staining intensity was reduced only after 15 days in culture. This reduction in strong ER staining was accompanied by a significant increase in cells showing moderate staining intensity. The reduction in strong ER staining was also reflected in a reduction of total ER protein, detectable by WB (Fig. 5A). E-cadherin was present at the membrane in the majority of the cells in both mono and co-cultures. To determine whether the level of membranous E-cadherin expression altered throughout the culture period, an image analysis algorithm was trained to recognise staining at four threshold levels: weak, medium, strong and negative (Fig. 5B). Quantification of membranous E-cadherin staining revealed that, at day 5, the level of membranous E-cadherin was similar in both mono- and co-cultures. In the mono-cultures however, E-cadherin localisation at the membrane increased over time as indicated by a significant increase in strong membranous staining, and a concomitant decrease in moderate membranous staining (Fig. 5B). In contrast, in the co-cultures, membranous E-cadherin was reduced at day 15, which is consistent with the observed changes in polarity in the co-cultures over time (Fig. 4D). It is of note that the inter-aggregate heterogeneity of E-cadherin staining by IHC was higher than that observed for the ER.

3.5. Tumour-stroma crosstalk within alginate microcapsules results in a pro-inflammatory environment and increased angiogenic response to MCF-7 cells

We next evaluated the production of cytokines in the microencapsulated monocultures, as well as in co-cultures over time (Fig. 6A and Supplementary figure S3). Mono-cultures of fibroblasts were used as controls. Supernatants from the extracellular fractions

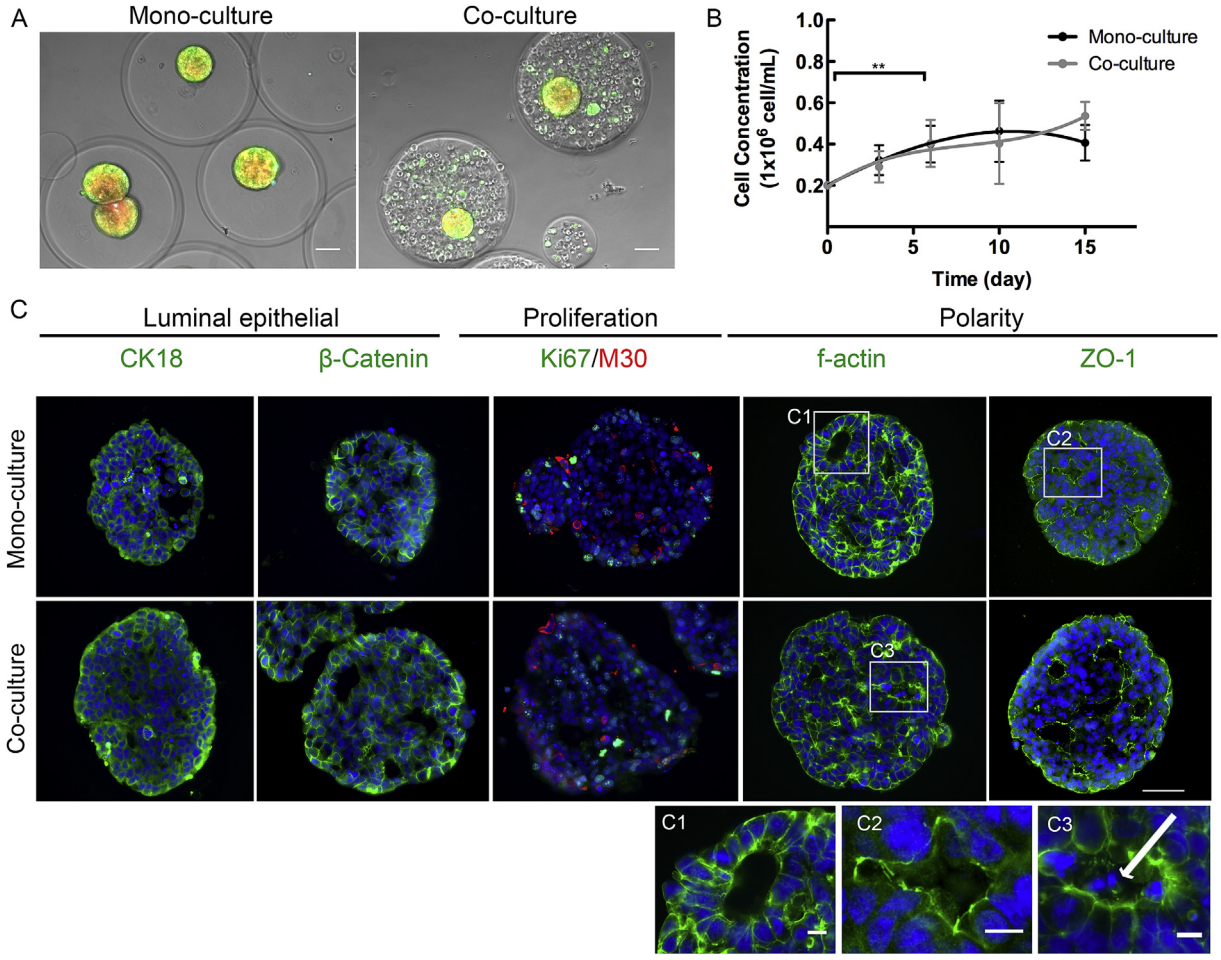

Fig. 2. Phenotypic characterization of microencapsulated mono and co-cultures. (A) Live/dead assay (FDA – green; ToPro3 – blue, respectively) of MCF-7 (red) tumour aggregates in mono and in co-culture with fibroblasts, at day 5. (B) Tumour cell concentration profile of mono and co-cultures along 15 days of culture; data are mean ± SD from four independent experiments; ** indicate significant difference with $p < 0.003$ by two way ANOVA statistics test. (C) Immunofluorescence microscopy of alginate microcapsules in 10 μm thick cryosections, at day 5, show mono-culture and co-culture aggregates in the upper and lower panels, respectively. From the left: Cytokeratin 18 (CK18; green), β-Catenin (green), Ki67 (green) and cleaved cytokeratin 18 (M30 cytodeath, red), f-actin (phalloidin; green), Zonula Occludens 1 (ZO-1, green) and DAPI (blue). (C1), (C2) and (C3) High magnification insets represent the regions indicated by the white squares. The white arrow indicates the pyknotic nuclei. Scale bars: 50 μm, 10 μm for high-magnification inset (For interpretation of the references to colour in this figure legend, the reader is referred to the web version of this article.).

of the culture supernatant (CS) and the microcapsule soluble fraction (MSF) were assayed for a panel of 36 cytokines.

Six cytokines were significantly higher in the co-cultures compared to the mono-cultures: Serpin-E1, CXCL1, IL8, IL6, IL1ra and sICAM-1 (Fig. 6A). Of these, the latter 2 appeared to be specifically retained inside the alginate microcapsules (Fig. 6A). No statistically significant differences were observed between co-cultures and fibroblast control cultures (Figure S3).

Since CXCL1, IL8 and sICAM-1 are known to promote angiogenesis [31–34], we analysed the impact of the co-culture system on the angiogenic potential of tumour cells at day 15 using a standard CAM assay. After removal of stromal cells, ECM and soluble factors, tumour cell aggregates from both types of culture were inoculated on the top of the CAM and incubated for 3 days. The results obtained show that the number of new blood vessels induced by the aggregates derived from co-cultures was higher than that induced by mono-cultures (Fig. 6B).

4. Discussion

Multiple attempts have been made in the last decade towards the improvement of *in vitro* preclinical models for cancer research [6]. Despite these efforts, most of the available models still fail to mimic several important aspects of the tumour microenvironment, and do not reflect the complexity of human tumours [6,7]. In addition, most *in vitro* experiments can only be carried out over short culture periods which, clearly, does not allow examination of longer term effects of the microenvironment or drug treatments on disease progression [35].

In this work we have developed a new strategy for *in vitro* reconstruction of tumour microenvironment complexity, using a robust culture system that allows long-term culture with continuous monitoring. This system uses alginate microencapsulation of epithelial tumour cell aggregates either alone or together with human fibroblasts. Tumour-stroma crosstalk was achieved by keeping cells in close proximity and by accumulation of ECM components and soluble factors in the alginate microcapsules. Culture progression over time could be evaluated due to the non-destructive sampling offered by this culture system.

Our results demonstrate that in microencapsulated aggregates, MCF-7 cells self-organized into tissue-like structures by establishing cell–cell contacts presumably via E-cadherin, by partial polarisation at the surface of multiple small lumina and inverse polarisation at the outer rim of the aggregate. Pyknotic nuclei were

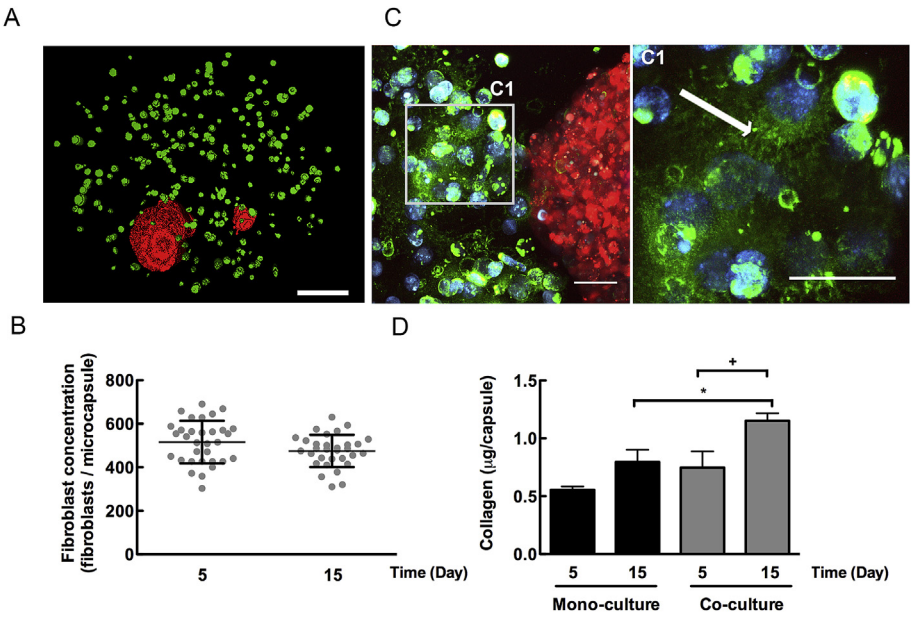

Fig. 3. Collagen accumulation within the stromal compartment. (A) Immunofluorescence microscopy of whole mount microencapsulated co-cultures of MCF-7 aggregates (red) and fibroblasts (vimentin – green), at day 5– 3D volume rendering of light sheet microscope (SPIM) images. (B) Number of fibroblasts *per* microcapsule, in co-cultures, at days 5 and 15 – images acquired by light sheet microscopy (SPIM); quantification method described in Ref. [21]. (C) Immunofluorescence microscopy of collagen I (green) in whole mount microencapsulated MCF-7 aggregates (red) and fibroblasts (blue), at day 5 – maximum intensity z-projection of 125 optical sections with 2 µm z-step by 2-photon microscopy. (C1) High magnification inset represents the region indicated by the white square. The white arrow indicates the collagen I fibres. (D) Total collagen quantification of mono and co-cultures, at days 5 and 15; data are mean ± SD from three independent experiments; * or + indicate significant difference with $p < 0.01$ by non-parametric Kruskal–Wallis statistics test (For interpretation of the references to colour in this figure legend, the reader is referred to the web version of this article.)

also detected within the lumina, suggestive of lumen formation via cell death and subsequent cavitation [36]. These features together with the relatively limited proliferative capacity are reminiscent of well differentiated human breast tumours of the luminal subtype or, indeed, the normal human breast epithelium [37,38]. The absence of myoepithelial cells with a resulting lack of basement membrane [39] may have contributed to the observed inverse polarity seen at the rims of the aggregates [40]. However, inverse polarity has also been described to occur *in vivo*, during tumorigenesis [41]. Therefore, we could recapitulate certain features of epithelial carcinomas such as breast by combining 3D aggregates with alginate microencapsulation. Other groups have shown that MCF-7 cells can polarise and maintain the luminal epithelial phenotype but only when cultured in Matrigel for 7 days [9] or in very long culture times in scaffold-free conditions (155 days) [42]. Similarly, we have also demonstrated that MCF-7 cells are unable to polarise when cultured over 5 days without scaffolds (i.e. non-microencapsulated), in our stirred-tank culture system although the luminal-epithelial phenotype was maintained (Figure S1). Overall our results demonstrate that aggregate microencapsulation in alginate, an inert scaffold, allows cell movement required for lumen formation and cell polarisation [37], by day 5 of culture.

We hypothesised that alginate entrapment of tumour cell aggregates together with human fibroblasts would further help reconstruction of the different aspects of the tumour microenvironment. Our results show the differential distribution of tumour and stromal cells. Epithelial tumour aggregates appear surrounded by fibroblasts, creating appropriately oriented “epithelial tumour” and “stromal” compartments within the alginate microcapsules. In contrast, when cultured without a scaffold, fibroblasts accumulated in the centre of the aggregates forming a core, as shown by us [26] and by others [43,44]. In cultures without scaffolds, the fibroblasts remained viable and maintained collagen expression, however the cellular organization did not resemble the human tumours where epithelial and stromal cells are organized into distinct compartments [3].

Imaging and quantification of collagen within the microcapsules demonstrated a significant increase of collagen deposition over the time in the co-cultures, suggesting that fibroblasts were playing their biologic role by actively producing collagen [45]. Furthermore, collagen type I appeared to be assembled into fibres within the stromal compartment, as typically observed in breast tissues [46,47]. Collagen is the major component of human breast stroma [48] and it is though that mammary epithelial cells migrate along type I collagen fibres during branching morphogenesis and tumour cell dissemination [49,50]. Additionally, other studies have shown that stiffer collagen matrices may promote mammary tumour cell dissemination [49,51]. Accordingly, many 3D tumour models have been developed using collagen type I matrices in order to determine the impact on tumour behaviour [2,6]. However, cell growth and migration is dependent on collagen physical properties, which, in turn, are greatly dependent on the type of cross-linking used [52]. For this reason, the *de novo* synthesis of collagen by stromal cells and its accumulation within the stromal compartment is a major advantage of the alginate microencapsulated culture system.

To further understand the role played by fibroblasts in our culture system, analysis of the profile of cytokines produced at early and late time points was carried out using cytokine arrays. Overall the results indicate increased secretion of pro-inflammatory cytokines, such as, IL6, IL8 and CXCL1 in the co-cultures. These pro-inflammatory cytokines have been linked with increased tumour aggressiveness, cell dissemination and angiogenesis [32]. Paradoxically, an anti-inflammatory cytokine (IL1ra) was also increased in the co-cultures. The reason for this is unclear but may be an intrinsic feedback mechanism that limits the effects of pro-inflammatory cytokines. Nevertheless, the overall balance of cytokines suggests a pro-inflammatory environment in the co-cultures. Furthermore, sICAM, a cytokine associated with tumour cell growth

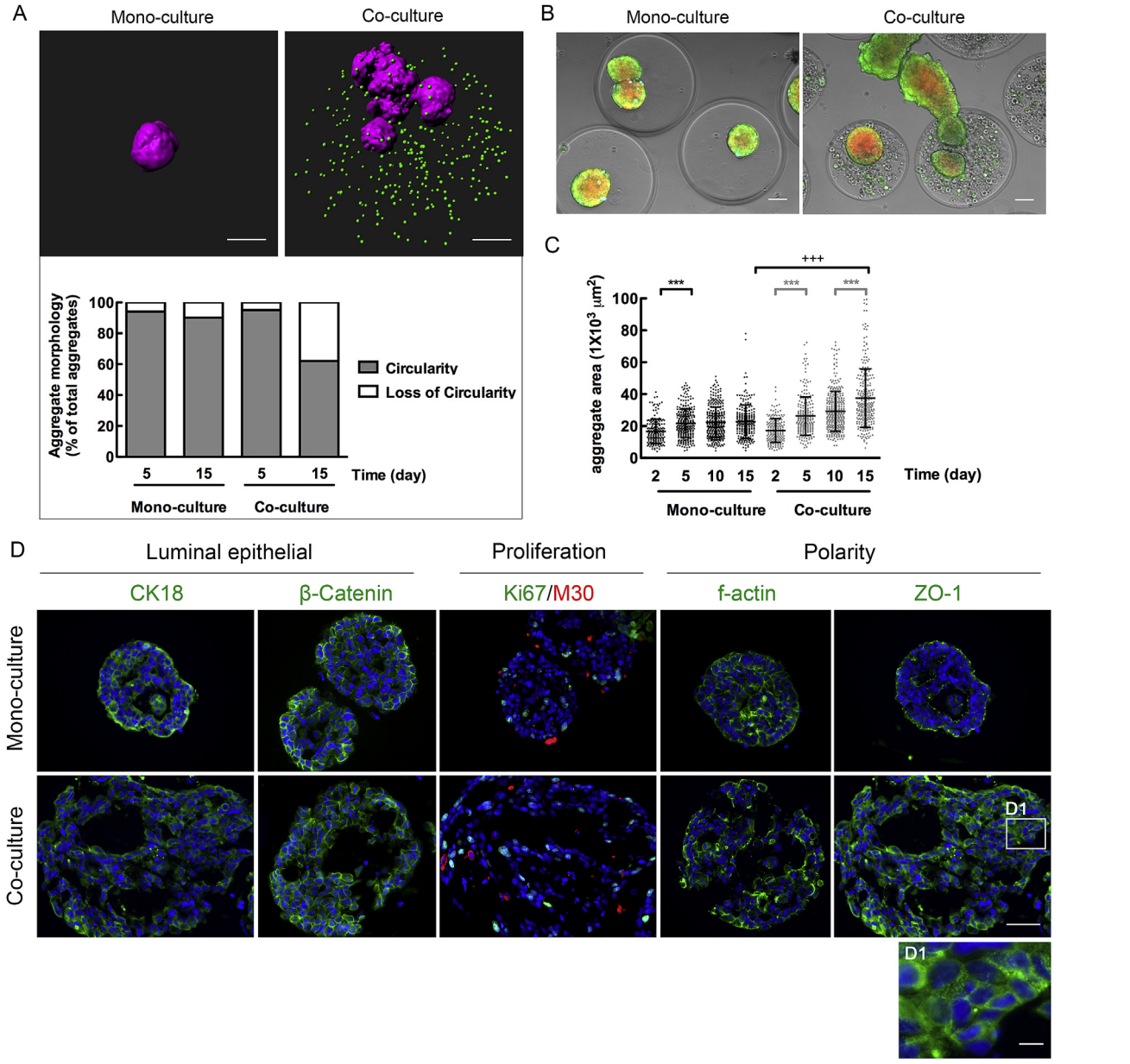

Fig. 4. Phenotypic characterization of long-term (up to 15 days) microencapsulated mono and co-cultures. (A) Immunofluorescence microscopy of whole mount microencapsulated MCF-7 aggregates (red) with or without fibroblasts (anti-vimentin – green), at day 15 – 3D volume rendering was carried out on images acquired with light sheet microscopy (SPIM); Morphologic analysis of approximately 100 aggregates from mono and co-cultures – images acquired using SPIM. (B) Live/dead assay (FDA – green; ToPro3 – blue, respectively) of MCF-7 (red) tumour aggregates in mono and in co-culture, at day 15. (C) Size distribution plot: aggregate surface area from mono and co-cultures, at days 2, 5, 10 and 15; data are mean ± SD from three independent experiments; *** and $^{+++}$ indicate significant difference with $p < 0.0001$ by the non-parametric Kruskal–Wallis statistics test. (D) Immunofluorescence microscopy of alginate microcapsules 10 µm thick cryosections, at day 15, show mono-culture and co-culture aggregates in the in the upper and lower panel, respectively. From the left: Cytokeratin 18 (CK18; green), β-Catenin (green), Ki67 (green) and cleaved cytokeratin 18 (M30 cytodeath, red), f-actin (phalloidin; green), Zonula Occludens 1 (ZO-1, green) and DAPI (blue). (D1) High magnification inset represents the region indicated by the white square. Scale bars: 50 µm, 10 µm for high-magnification inset (For interpretation of the references to colour in this figure legend, the reader is referred to the web version of this article.).

and angiogenesis [34] was higher in the co-cultures and specifically accumulated in the alginate microcapsule. It is well known that a shift in the cytokine balance from an anti- to a pro-inflammatory environment may lead to chronic inflammation that consequently promotes tumour progression [53,54]. Our results recapitulate this inflammatory shift, which strengthens our model as a good alternative to study tumour-stroma crosstalk mechanisms.

The non-destructive sampling allowed us to continuously monitor the effect of the reconstructed microenvironment on culture progression throughout the culture time. By day 15, tumour aggregates in co-cultures had an altered phenotype that was not observed in mono-cultures. Analysis of aggregate morphology by SPIM-FLUID microscopy [21] demonstrated that approximately 40% of the aggregates in co-culture had become irregular in shape and had lost their circularity. In contrast 90% of the aggregates in the mono-cultures retained their circularity. This change in shape in the co-cultures resulted in increased aggregate surface area and was accompanied by aggregate cell migration out of the microcapsules. The directionality of aggregate migration accompanied by the stabilization of tumour cell concentration, is suggestive of an event of collective cell migration rather than the cell movement associated with expansive cell growth [50]. Ductal elongation, such

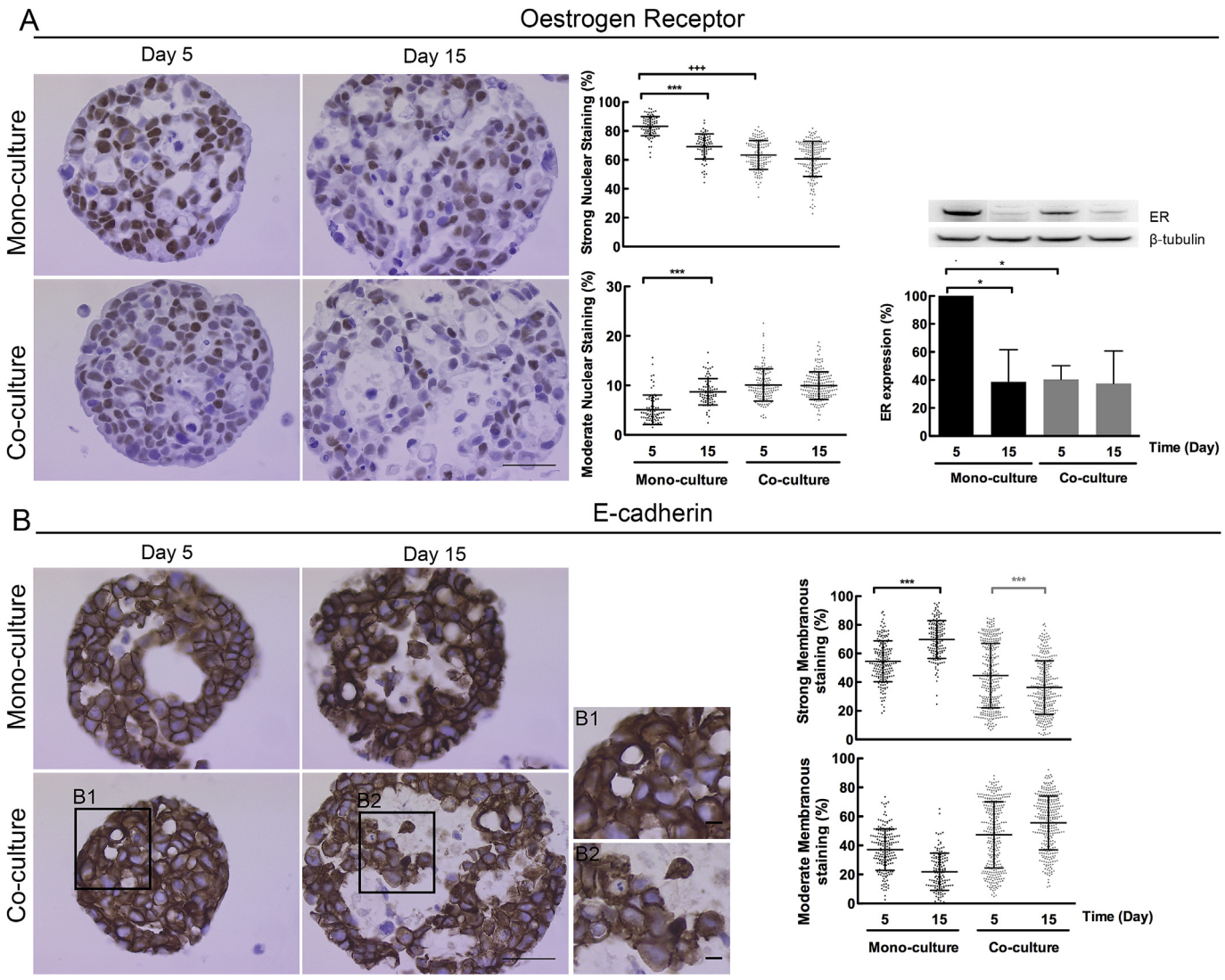

Fig. 5. Molecular characterization of ER and E-cadherin in long-term (day 15) microencapsulated mono and co-cultures. (A) Immunohistochemistry staining of 3 μm thick paraffin sections of alginate microcapsules taken at days 5 and 15, show mono-culture and co-culture aggregates stained with (A) Oestrogen Receptor (ER); and (B) E-cadherin, and respective quantification of nuclear ER and membranous E-cadherin. (B1) and (B2) High magnification inset represents the region indicated by the black square. ER quantification by Western Blot from total protein extracts. Data are mean ± SD from two independent experiments; * indicate significant difference with $p < 0.01$* and ***or $^{+++}$ indicate significant difference with $p < 0.0001$, both by a two way ANOVA statistics test. Scale bar: 50 μm (For interpretation of the references to colour in this figure legend, the reader is referred to the web version of this article.).

as that occurring during breast morphogenesis, is described as a directional collective migration process [37], which might explain the observed directionality in aggregate migration from the microcapsules. The accumulation of collagen exclusively in the stromal compartment of co-cultures might be enough to stimulate collective tumour cell migration. Furthermore, collective cell migration typically occurs in carcinomas and has been described as a crucial step in the disease progression towards metastatic cancer [55].

The altered aggregate morphology and loss of cell polarity, observed at day 15 in co-cultures, appears to be heralded by reduced nuclear expression of ER which could be seen as early as day 5 of co-culture compared to the aggregates in mono-culture. The reasons underlying this early reduction in ER expression are not, as yet, known but we speculate that reduction of signalling through this receptor may be necessary before other phenotypic changes can occur. Nuclear ER expression also declined in the mono-cultures but at a much slower rate and was only apparent after 15 days of culture. It is possible that the aggregates in the mono-cultures would also have undergone a change in behaviour and phenotype similar to that seen in the co-cultures if they had been maintained in culture for long enough. This difference between mono and co-culture suggests that fibroblasts are accelerating ER depletion, as previously demonstrated by others [56]. ER^{+} breast cancers are described to present high frequency of disease relapse associated with metastasis and drug resistance, despite an initial response to endocrine therapy [27,28]. Loss of hormone dependency accompanied by altered sub-cellular localization of E-cadherin and altered cell polarity have been described as common features of more aggressive and invasive breast cancers [57–59]. Quantification of membranous E-cadherin revealed a very high percentage of aggregate heterogeneity in co-cultures compared to mono-cultures, which was similar to the heterogeneity in aggregate circularity, although the correlation between these two parameters has not been addressed. The reduction in E-cadherin membrane staining could contribute to the observed loss of

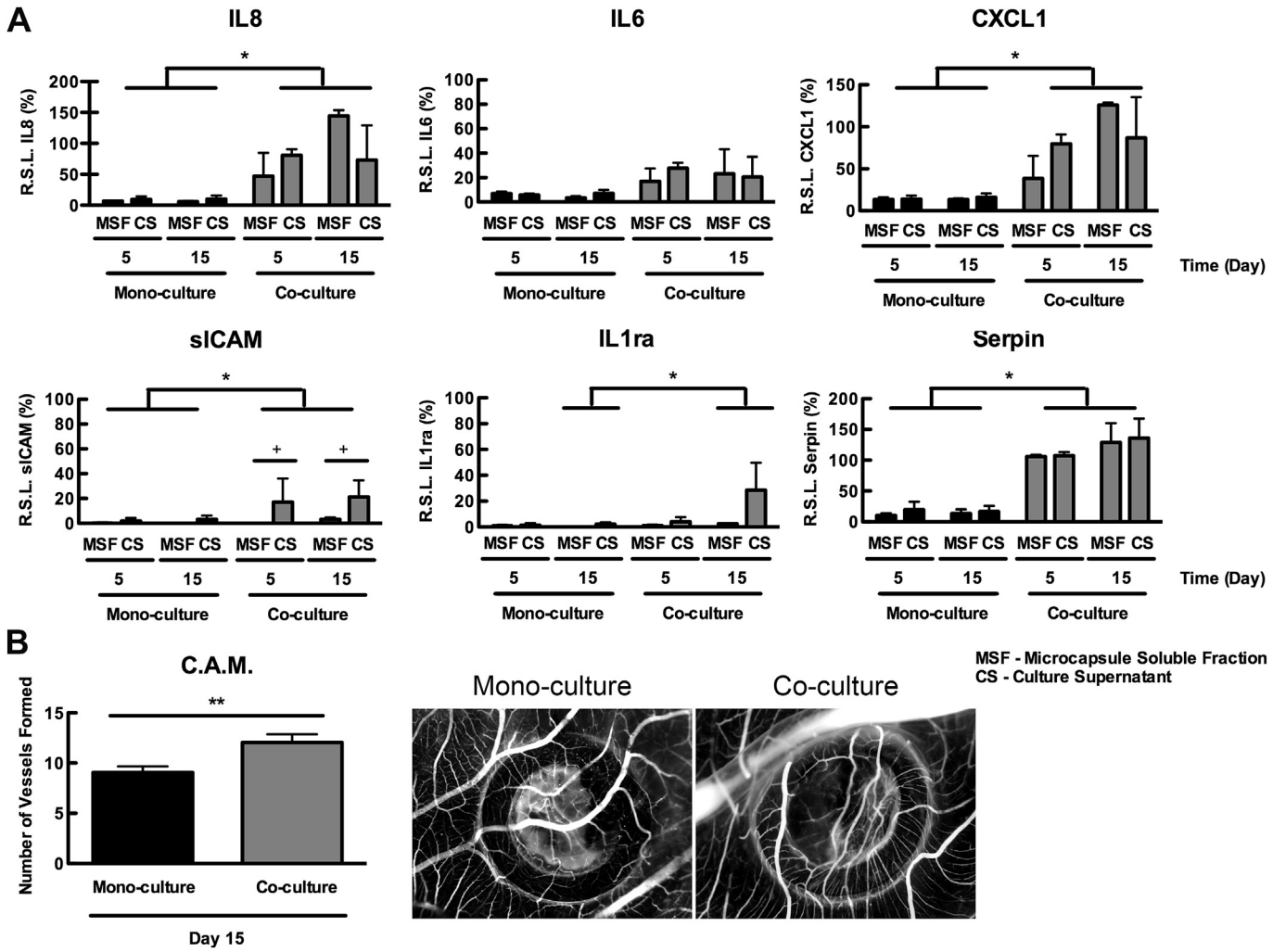

Fig. 6. Characterization of the inflammatory environment and angiogenic potential of tumour cells microencapsulated in co-cultures. (A) Cytokine arrays of mono and co-cultures from days 5 and 15, were performed for both culture and capsule supernatant. Data are mean ± SD from two independent experiments. * or $^{+}$ indicate significant difference with $p < 0.01$ by a non-parametric Man-Whitney U statistics Test (two-tailed p-value). Microencapsulated mono-cultures of fibroblasts were used as controls. (B) Quantification and representative images of Chick Chorioallantoic Membrane (CAM) Assays of tumour aggregates from both mono and co-cultures, at day 15. Vessels with less than 15 μm of diameter, growing in a wheel shape manner towards the inoculation area, were quantified as newly formed vessels. Data are mean ± SD from 18 eggs. ** indicate significant difference with $p < 0.001$ by a t- Test (two-tailed p-value).

aggregate circularity. Furthermore, the intra-culture heterogeneity observed in co-cultures is critical, since it may recapitulate the intra-tumour heterogeneity observed in human tumours [50].

The angiogenic potential of both mono and co-cultures was analysed by Chick Chorioallantoic Membrane (CAM) assay. Our results demonstrate that, by day 15, tumour aggregates from co-cultures have a higher capacity to induce angiogenesis, which was indicated by the significant increase in the number of new radial blood vessels formed towards the aggregates from co-cultures, when compared to those from mono-cultures. This increase might be related to the increased expression of pro-angiogenic cytokines in co-cultures, such as CXCL1 and IL8 in the co-cultures [31–33]. Overall, our results show that tumour cells were indeed educated by the stroma, since the new blood vessels formed in the CAM assay were induced only by those tumour cells that had been cultured for 15 days within the reconstructed tumour microenvironment.

In conclusion, we have developed a robust and versatile model system for long-term *in vitro* recapitulation of tumour-stroma crosstalk, via reconstruction of key aspects of the tumour microenvironment such as *de novo* synthesis and accumulation of ECM and cytokines, and allowing continuous monitoring of tumour progression events *in vitro*. Entrapment of tumour cells and fibroblasts in an inert scaffold allowed *de novo* synthesis and deposition of ECM by the cells, and the accumulation of soluble factors, promoting tumour-stroma crosstalk. This model system is transferrable to other types of tumour cells and provides a new tool for further understanding tumour progression and drug resistance mechanisms using either cell lines or patient-derived primary cultures. In addition, it is easily transferable to industry for feeding high-throughput systems or miniaturised bioreactors used for drug development and target validation.

Acknowledgements

We gratefully acknowledge Dr Cathrin Brisken for the supply of the MCF-7-dsRED cell line within the scope of the IMI-funded project PREDECT and for valuable advice. We are grateful to the PREDECT consortium partners, especially to Dr John Hickman, Dr Juha Klefström and Dr Georgios A. Sflomos for fruitful discussions. We also thank Dr Joana Paredes for critical advice. We acknowledge support from the Innovative Medicines Initiative Joint Undertaking

(IMI grant agreement n° 115188), resources composed of financial contribution from EU – FP7 and EFPIA companies in kind contribution. We also acknowledge support from MINECO/FEDER project BIO2014-59614-JIN and from Fundação para a Ciência e Tecnologia (FCT), Portugal (EXPL/BBB-IMG/0363/2013); MFE is the recipient of a PhD fellowship from FCT (SFRH/BD/52208/2013).

Appendix A. Supplementary data

Supplementary data related to this article can be found at http://dx.doi.org/10.1016/j.biomaterials.2015.11.030.

References

[1] M.J. Bissell, W.C. Hines, Why don't we get more cancer? A proposed role of the microenvironment in restraining cancer progression, Nat. Med. 17 (2011) 320–329.
[2] K.-V. Nguyen-Ngoc, K.J. Cheung, A. Brenot, E.R. Shamir, R.S. Gray, W.C. Hines, et al., ECM microenvironment regulates collective migration and local dissemination in normal and malignant mammary epithelium, Proc. Natl. Acad. Sci. U. S. A. 109 (2012) E2595–E2604.
[3] Z.I. Khamis, Z.J. Sahab, Q.-X.A. Sang, Active roles of tumor stroma in breast cancer metastasis, Int. J. Breast Cancer 2012 (2012) 574025–574035.
[4] K. Kessenbrock, V. Plaks, Z. Werb, Matrix metalloproteinases: regulators of the tumor microenvironment, Cell 141 (2010) 52–67.
[5] 19, Cancer Associated Fibroblasts–More Than Meets The Eye, 2013, pp. 447–453.
[6] B. Weigelt, C.M. Ghajar, M.J. Bissell, The need for complex 3D culture models to unravel novel pathways and identify accurate biomarkers in breast cancer, Adv. Drug Deliv. Rev. 69–70 (2014) 42–51.
[7] C. Hirt, A. Papadimitropoulos, M.G. Muraro, V. Mele, E. Panopoulos, E. Cremonesi, et al., Bioreactor-engineered cancer tissue-like structures mimic phenotypes, gene expression profiles and drug resistance patterns observed in vivo, Biomaterials 62 (2015) 138–146.
[8] J.E. Ekert, K. Johnson, B. Strake, J. Pardinas, S. Jarantow, R. Perkinson, et al., Three-dimensional lung tumor microenvironment modulates therapeutic compound responsiveness in vitro–implication for drug development, PLoS ONE 9 (2014) e92248.
[9] C.E. Smart, B.J. Morrison, J.M. Saunus, A.C. Vargas, P. Keith, L. Reid, et al., In vitro analysis of breast cancer cell line tumourspheres and primary human breast epithelia mammospheres demonstrates inter- and intrasphere heterogeneity, PLoS ONE 8 (2013) e64388.
[10] P. Mafi, S. Hindocha, R. Mafi, W.S. Khan, Evaluation of biological protein-based collagen scaffolds in cartilage and musculoskeletal tissue engineering–a systematic review of the literature, Curr. Stem Cell Res. Ther. 7 (2012) 302–309.
[11] K.E. Sung, D.J. Beebe, Microfluidic 3D models of cancer, Adv. Drug Deliv. Rev. 79–80 (2014) 68–78.
[12] K. Chwalek, M.V. Tsurkan, U. Freudenberg, C. Werner, Glycosaminoglycan-based hydrogels to modulate heterocellular communication in in vitro angiogenesis models, Sci. Rep. 4 (2014) 4414.
[13] T. Andersen, P. Auk-Emblem, M. Dornish, 3D cell culture in alginate hydrogels, Microarrays 4 (2015) 133–161, 2015;4:133–61.
[14] J. Sun, H. Tan, Alginate-based biomaterials for regenerative medicine applications, Materials 6 (2013) 1285–1309.
[15] K. Alessandri, B.R. Sarangi, V.V. Gurchenkov, B. Sinha, T.R. Kießling, L. Fetler, et al., Cellular capsules as a tool for multicellular spheroid production and for investigating the mechanics of tumor progression in vitro, Proc. Natl. Acad. Sci. U. S. A. 110 (2013) 14843–14848.
[16] S.-F. Lan, B. Starly, Alginate based 3D hydrogels as an in vitro co-culture model platform for the toxicity screening of new chemical entities, Toxicol. Appl. Pharmacol. 256 (2011) 62–72.
[17] L.C. Kimlin, G. Casagrande, V.M. Virador, In vitro three-dimensional (3D) models in cancer research: an update, Mol. Carcinog. 52 (2013) 167–182.
[18] J.W. Haycock, 3D cell culture: a review of current approaches and techniques, Methods Mol. Biol. 695 (2011) 1–15.
[19] S.P. Rebelo, R. Costa, M. Estrada, V. Shevchenko, C. Brito, P.M. Alves, HepaRG microencapsulated spheroids in DMSO-free culture: novel culturing approaches for enhanced xenobiotic and biosynthetic metabolism, Arch. Toxicol. (2014) 1–12.
[20] D. Simão, C. Pinto, S. Piersanti, A. Weston, C.J. Peddie, A.E.P. Bastos, et al., Modeling human neural functionality in vitro: three-dimensional culture for dopaminergic differentiation, Tissue Eng. Part A 21 (2015) 654–668.
[21] E.J. Gualda, H. Pereira, T. Vale, M.F. Estrada, C. Brito, N. Moreno, SPIM-fluid: open source light-sheet based platform for high-throughput imaging, Biomed. Opt. Express 6 (2015) 4447–4456.
[22] E.J. Gualda, T. Vale, P. Almada, J.A. Feijó, G.G. Martins, N. Moreno, OpenSpinMicroscopy: an open-source integrated microscopy platform, Nat. Methods 10 (2013) 599–600.
[23] J. Schindelin, I. Arganda-Carreras, E. Frise, V. Kaynig, M. Longair, T. Pietzsch, et al., Fiji: an open-source platform for biological-image analysis, Nat. Methods 9 (2012) 676–682.
[24] E.J. Davies, V. Marsh Durban, V. Meniel, G.T. Williams, A.R. Clarke, PTEN loss and KRAS activation leads to the formation of serrated adenomas and metastatic carcinoma in the mouse intestine, J. Pathol. 233 (2014) 27–38.
[25] A. Sakai, M. Ohshima, N. Sugano, K. Otsuka, K. Ito, Profiling the cytokines in gingival crevicular fluid using a cytokine antibody array, J. Periodontol. 77 (2006) 856–864.
[26] V.E. Santo, M.F. Estrada, S.P. Rebelo, I. Silva, A.C. Pinto, S.C. Veloso, et al., Adaptable stirred-tank culture strategies for large scale production of spheroid-based tumor cell models, *J. Biotechnol*, accepted.
[27] N. Yoshida, Y. Omoto, A. Inoue, H. Eguchi, Y. Kobayashi, M. Kurosumi, et al., Prediction of prognosis of estrogen receptor-positive breast cancer with combination of selected estrogen-regulated genes, Cancer Sci. 95 (2004) 496–502.
[28] M.P.V. Shekhar, S. Santner, K.A. Carolin, L. Tait, Direct involvement of breast tumor fibroblasts in the modulation of tamoxifen sensitivity, Am. J. Pathol. 170 (2007) 1546–1560.
[29] D.L. Holliday, V. Speirs, Choosing the right cell line for breast cancer research, Breast Cancer Res. 13 (2011) 215.
[30] S.M. Kakkad, M. Solaiyappan, P. Argani, S. Sukumar, L.K. Jacobs, D. Leibfritz, et al., Collagen I fiber density increases in lymph node positive breast cancers: pilot study, J. Biomed. Opt. 17 (2012) 116017–116027.
[31] J.K. Singh, B.M. Simões, S.J. Howell, G. Farnie, R.B. Clarke, Recent advances reveal IL-8 signaling as a potential key to targeting breast cancer stem cells, Breast Cancer Res. 15 (2013) 210.
[32] P. DelNero, M. Lane, S.S. Verbridge, B. Kwee, P. Kermani, B. Hempstead, et al., 3D culture broadly regulates tumor cell hypoxia response and angiogenesis via pro-inflammatory pathways, Biomaterials 55 (2015) 110–118.
[33] S. Acharyya, T. Oskarsson, S. Vanharanta, S. Malladi, J. Kim, P.G. Morris, et al., A CXCL1 paracrine network links cancer chemoresistance and metastasis, Cell 150 (2012) 165–178.
[34] C. Chen, C.A. Duckworth, B. Fu, D.M. Pritchard, J.M. Rhodes, L.-G. Yu, Circulating galectins -2, -4 and -8 in cancer patients make important contributions to the increased circulation of several cytokines and chemokines that promote angiogenesis and metastasis, Br. J. Cancer 110 (2014) 741–752.
[35] C. Unger, N. Kramer, A. Walzl, M. Scherzer, M. Hengstschläger, H. Dolznig, Modeling human carcinomas: physiologically relevant 3D models to improve anti-cancer drug development, Adv. Drug Deliv. Rev. 79–80 (2014) 50–67.
[36] D.M. Bryant, K.E. Mostov, From cells to organs: building polarized tissue, Nat. Rev. Mol. Cell Biol. 9 (2008) 887–901.
[37] A.J. Ewald, A. Brenot, M. Duong, B.S. Chan, Z. Werb, Collective epithelial migration and cell rearrangements drive mammary branching morphogenesis, Dev. Cell 14 (2008) 570–581.
[38] M.J. Piccart-Gebhart, New developments in hormone receptor-positive disease, Oncologist 16 (Suppl 1) (2011) 40–50.
[39] T. Gudjonsson, L. Rønnov-Jessen, R. Villadsen, F. Rank, M.J. Bissell, O.W. Petersen, Normal and tumor-derived myoepithelial cells differ in their ability to interact with luminal breast epithelial cells for polarity and basement membrane deposition, J. Cell Sci. 115 (2002) 39–50.
[40] N. Akhtar, C.H. Streuli, An integrin-ILK-microtubule network orients cell polarity and lumen formation in glandular epithelium, Nat. Cell Biol. 15 (2013) 17–27.
[41] S.A. Adams, M.E.F. Smith, G.P. Cowley, L.A. Carr, Reversal of glandular polarity in the lymphovascular compartment of breast cancer, J. Clin. Pathol. 57 (2004) 1114–1117.
[42] J.B. do Amaral, M.S. Urabayashi, G.M. Machado-Santelli, Cell death and lumen formation in spheroids of MCF-7 cells, Cell Biol. Int. 34 (2010) 267–274.
[43] P. Kaur, B. Ward, B. Saha, L. Young, S. Groshen, G. Techy, et al., Human breast cancer histoid: an in vitro 3-dimensional co-culture model that mimics breast cancer tissue, J. Histochem Cytochem 59 (2011) 1087–1100.
[44] C. Angelucci, G. Maulucci, G. Lama, G. Proietti, A. Colabianchi, M. Papi, et al., Epithelial-stromal interactions in human breast cancer: effects on adhesion, plasma membrane fluidity and migration speed and directness, PLoS ONE 7 (2012) e50804.
[45] B. Weigelt, M.J. Bissell, Unraveling the microenvironmental influences on the normal mammary gland and breast cancer, Semin. Cancer Biol. 18 (2008) 311–321.
[46] B. Alberts, A. Johnson, J. Lewis, D. Morgan, M. Raff, K. Roberts, et al., Molecular Biology of the Cell, sixth ed., Garland Science, 2014.
[47] S.M. Kakkad, M. Solaiyappan, B. O'Rourke, I. Stasinopoulos, E. Ackerstaff, V. Raman, et al., Hypoxic tumor microenvironments reduce collagen I fiber density, Neoplasia 12 (2010) 608–617.
[48] M.W. Conklin, P.J. Keely, Why the stroma matters in breast cancer: insights into breast cancer patient outcomes through the examination of stromal biomarkers, Cell Adhes. Migr. 6 (2012) 249–260.
[49] T.R. Cox, J.T. Erler, Remodeling and homeostasis of the extracellular matrix: implications for fibrotic diseases and cancer, Dis. Model. Mech. 4 (2011) 165–178.
[50] P. Friedl, S. Alexander, Cancer invasion and the microenvironment: plasticity and reciprocity, Cell 147 (2011) 992–1009.
[51] C. Bonnans, J. Chou, Z. Werb, Remodelling the extracellular matrix in development and disease, Nat. Rev. Mol. Cell Biol. 15 (2014) 786–801.
[52] G. Vaissiere, B. Chevallay, D. Herbage, O. Damour, Comparative analysis of different collagen-based biomaterials as scaffolds for long-term culture of human fibroblasts, Med. Biol. Eng. Comput. 38 (2000) 205–210.

[53] A. Yuzhalin, A. Kutikhin, Interleukins in Cancer Biology, Academic Press, 2014.
[54] V.R. Zellmer, S. Zhang, Evolving concepts of tumor heterogeneity, Cell & Biosci. 4 (2014) 69.
[55] K.J. Cheung, E. Gabrielson, Z. Werb, A.J. Ewald, Collective invasion in breast cancer requires a conserved basal epithelial program, Cell 155 (2013) 1639–1651.
[56] S.E. Holton, A. Bergamaschi, B.S. Katzenellenbogen, R. Bhargava, Integration of molecular profiling and chemical imaging to elucidate fibroblast-microenvironment impact on cancer cell phenotype and endocrine resistance in breast cancer, PLoS ONE 9 (2014) e96878.
[57] J.L.L. Robinson, K.A. Holmes, J.S. Carroll, FOXA1 mutations in hormone-dependent cancers, Front. Oncol. 3 (2013) 20.
[58] A.M. Scherbakov, O.E. Andreeva, V.A. Shatskaya, M.A. Krasil'nikov, The relationships between snail1 and estrogen receptor signaling in breast cancer cells, J. Cell Biochem. 113 (2012) 2147–2155.
[59] Y.J. Suh, J.H. Chang, C.S. Chun, Restoration of hormone dependency in estrogen receptor-lipofected MDA-MB-231 human breast cancer cells, J. Korean Cancer Assoc. 31 (3) (1999).